Overtwisted, Resolvable Carbon Nanotube Yarn Entanglement as Strain Sensors and Rotational Actuators

Yibin Li,[†,‡] Yuanyuan Shang,[†,‡] Xiaodong He,[†,*] Qingyu Peng,[†] Shanyi Du,[†] Enzheng Shi,[‡] Shiting Wu,[‡] Zhen Li,[§] Peixu Li,[§] and Anyuan Cao[‡,*]

[†]Centre for Composite Materials and Structures, Harbin Institute of Technology, Harbin 150080, P. R. China, [‡]Department of Materials Science and Engineering, College of Engineering, Peking University, Beijing 100871, P. R. China, and [§]Department of Mechanical Engineering, Tsinghua University, Beijing 100084, P. R. China

ABSTRACT Introducing twists into carbon nanotube yarns could produce hierarchical architectures and extend their application areas. Here, we utilized such twists to produce elastic strain sensors over large strain (up to 500%) and rotation actuators with high energy density. We show that a helical nanotube yarn can be overtwisted into highly entangled, macroscopically random but locally organized structures, consisting of mostly double-helix segments intertwined together. Pulling the yarn ends completely resolved the entanglement in an elastic and reversible way, yielding large tensile strains with linear change in electrical resistance. Resolving an entangled yarn and releasing its twists could simultaneously rotate a heavy object (30 000 times the yarn weight) for more than 1000 cycles at high speed. The rotational actuation generated from a single entangled yarn produced energy densities up to 8.3 kJ/kg, and maintained similar capacity during repeated use. Our entangled CNT yarns represent a complex self-assembled system with applications as large-range strain sensors and robust rotational actuators.

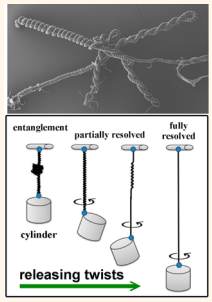

KEYWORDS: carbon nanotube yarn · entanglement · twist · stain sensor · rotational actuator

Light-weight, strong, conductive carbon nanotube (CNT) yarns have attracted intensive interest in various research areas from flexible supercapacitor or battery electrodes to high performance artificial muscles. Yet previous study has mainly focused on relatively simple structures such as straight-shape yarns. Given the one-dimensional structure, it is possible to further create more complex architectures utilizing the strength and flexibility of nanotubes, which may extend application areas. CNT yarns are typically made by spinning a large number of nanotubes and introducing twists to generate strong van der Waals forces among nanotubes,[1−7] and have shown a number of potential applications such as tough fibers, conducting wires and electrodes, sensors and actuators.[8−19] More recently, by controlling the twisting direction and guest infiltration, tensile and torsional actuators that can be triggered by versatile ways (electrically, chemically, photonically) have been demonstrated.[14−19] It shows that deliberate modification on the yarn structure is a powerful way to bring novel properties and extend application areas. Owing to the mechanical strength and flexibility, a straight CNT yarn can be overtwisted and form regular helical loops resulting in single- and double-helix structures, as reported by our group.[20,21] During the initial process of spinning, twists are applied to individual nanotubes and hold them tightly, resulting in a straight dense yarn. After that, upon continued spinning, more twists can be incorporated into the yarn by microscopic structural deformation (*e.g.*, coiling) leading to a helical or spiral morphology.[20,21]

Here, we show that extensive twists can be introduced into a thin flexible CNT yarn by spinning, resulting in a random entanglement analogous to a mingled and entangled rope. Compared with straight or helical yarns with relatively simple configurations, in the present work we explore the behavior of such entangled CNT yarns with a much higher level of structural hierarchy and complexity formed under an ultimate overtwisting condition. We find that the yarn entanglement can be fully resolved and stretched to very large tensile strains, with elastic strain recovery (due to the presence of twists) and linear change in

* Address correspondence to xdhe@hit.edu.cn, anyuan@pku.edu.cn.

Received for review July 3, 2013 and accepted August 20, 2013.

Published online August 20, 2013
10.1021/nn403400c

electrical resistance. Furthermore, the twists in an entanglement can be released under predefined tensile loads to rotate a heavy object at high speed for many cycles with a higher output energy density. Our results demonstrate a complex twist-induced yarn structure and its potential applications as superelastic strain sensors and rotational actuators.

RESULTS AND DISCUSSION

The fabrication of yarn entanglements was based on the conventional dry-spinning technique widely used for spinning straight CNT yarns and fibers,[4,5] while here we introduced high degree overtwisting to change the yarn morphology. Overtwisting is a simple and controllable method to form single-helix and double-helix structures along the yarn, as reported previously.[20,21] The entire process involved several steps that converted the material shape from a straight yarn to a helical yarn with close arranged loops, and ultimately a highly entangled agglomerate by continuous spinning (illustrated in Figure 1a). Single-walled CNT films were synthesized by chemical vapor deposition (CVD) using ferrocene and xylene as the catalyst and carbon precursor with a small addition of sulfur at a reaction temperature of 1160 °C, and CNT yarns were fabricated by spinning as-grown freestanding CNT films (see Methods for details). The two ends of a single yarn were fixed on an electric motor and a metal block, respectively, and twists were incorporated into the yarn from the rotating motor. With increasing overtwisting, self-assembled double-helix structures evolved at random positions along the yarn length and gradually intertwined together to form various configurations. An initially long yarn finally shrank into a small aggregation containing extensive twists; however, the structure remained stable even when the yarn ends were not fixed, indicating that all the twists were self-interlocked within the entanglement.

Scanning electron microscopy (SEM) characterization shows that as-produced CNT entanglements have various configurations, consisting of mostly double-helix segments with different sizes and other helical structures mixed together (Figure 1b,c). These double-helix and other segments form at the middle portion of a single yarn, protruding toward random directions. Formation of different morphologies is due to the nucleation of those branches at arbitrary positions, and more controlled structure might be obtained by predefining the nucleation sites. Many unique structures are observed, for example, a double-helix wrapped by another spiral helix (Figure 1d). Enlarged views on the center portions reveal very complex and intertwined structures that have not been observed in previously reported CNT yarns (Figure 1e−g). There are aligned wrinkles present on the loop surface which represent the traces of overtwisting (Figure 1f). The entangled portion is stable and does not unravel in air or liquid. A yarn with smaller diameter (<20 μm) usually results in a denser configuration compared with larger diameter yarns (Supporting Information, Figure S1). On the basis of the CNT bundle diameter and intertube distance, the yarn has a packing density (percentage of CNT volume) of less than 30% and maintains a porous structure after such extensive twisting (Figure S2). Formation of these highly entangled features without breaking the structure is owing to the extreme flexibility of our single-walled nanotube yarns.

The complex entanglement can be resolved into a straight (single-helical) yarn by pulling the exposed yarn ends toward opposite directions (Figure 1h). The straightened yarn length typically increases by several folds in this way. Thus, the intertwined portion is not dead-locked and fully resolvable upon uniaxial stretching. When the yarn ends are tethered by grips, the twists cannot be released during stretching and the straightened yarn tend to shrink into an entanglement again upon load removal. Unless one of the ends is free for rotation, a partial or fully resolved yarn still contains helical loops or twists locally. The entangled yarn shows elastic recovery during relatively slow or fast stretching for many cycles.

Mechanical (tensile) tests were carried out by gripping the two yarn ends and stretching the entanglement into a predefined strain, repeatedly (illustrated in Figure 2a). In this setup, the yarn ends are tethered and cannot rotate freely; therefore, the twists are maintained, which is important for elastic recovery during unloading. A typical stress−strain ($\sigma-\varepsilon$) curve until fracture shows ultralarge failure strain (ε = 985%) due to the yarn straightening with a tensile strength of about 100 MPa (Figure 2b). Tensile strain is defined as the stretched yarn length divided by the initial entanglement span, and typically the strain values are very large as seen in Figure 1h. The ultimate tensile strength depends on a few factors including the yarn diameter, uniformity and existing stress concentration sites due to high-degree overtwisting. There are two distinct stages during loading, a long plateau (ε = 0−800%) corresponding to entanglement resolving and a steep rising of stress due to ultimate yarn stretching until fracture (ε = 800−985%). The first stage is characterized by many fluctuations indicating high instability caused by the entangled structure, while the second stage (on resolved single-helix yarn) is rather smooth with increased slope. We have set a tensile strain of 500% to investigate the behavior of the entanglement within the first (elastic) stage. Many pronounced stress peaks occur during loading, which corresponds to the resolving events of the complex entanglement consisting of mostly double-helix segments (Figure 2c). Furthermore, $\sigma-\varepsilon$ curves from the second cycle to the following cycles are highly consistent in which the stress peaks occur at similar positions with comparable intensities, while the first cycle is different from others.

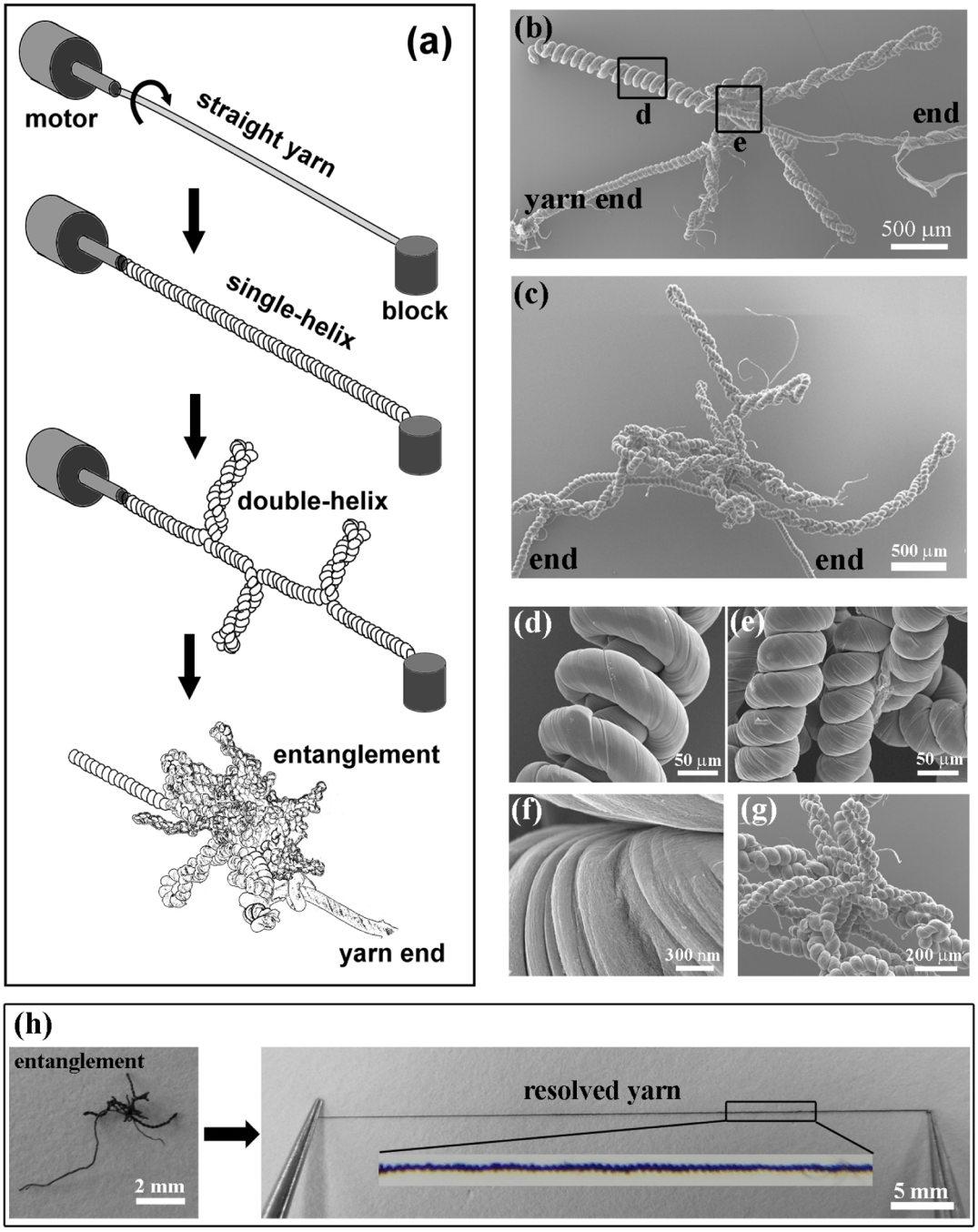

Figure 1. Fabrication and characterization of CNT entanglements. (a) Illustration of the spinning process in which a straight yarn with two ends fixed was overtwisted continuously into a helical shape, and finally an entanglement. (b and c) SEM images of two CNT entanglements with different morphologies. The exposed yarn ends are indicated, which can be stretched to resolve the entanglement. (d and e) Enlarged views of the entangled portions within the entanglement shown in (b). (f) Close view of the yarn surface. (g) Enlarged view of the entanglement shown in (c). (h) Images of an as-spun CNT entanglement and the resolved straight single-helix yarn by pulling the two yarn ends using tweezers.

Microstructure analysis reveals that the entanglement reorganizes its structure after the first cycle, and then remains the same configuration during subsequent cycles (Figure S3). Sometimes we observe that a complex entanglement reorganizes into a relatively simple structure consisting of two double-helix segments. This structural reorganization is due to different loading conditions between the fabrication process (a constant weight was fixed to one of the yarn end, Figure 1a) and mechanical testing (with changing load/stress, Figure 2c). Under the same loading condition, the entanglement structure remains stable and reversible starting from the second cycle, resulting in consistent stress peaks (Figure 2c). Although it is difficult to predefine a particular entanglement morphology, it might be possible to utilize the loading condition to

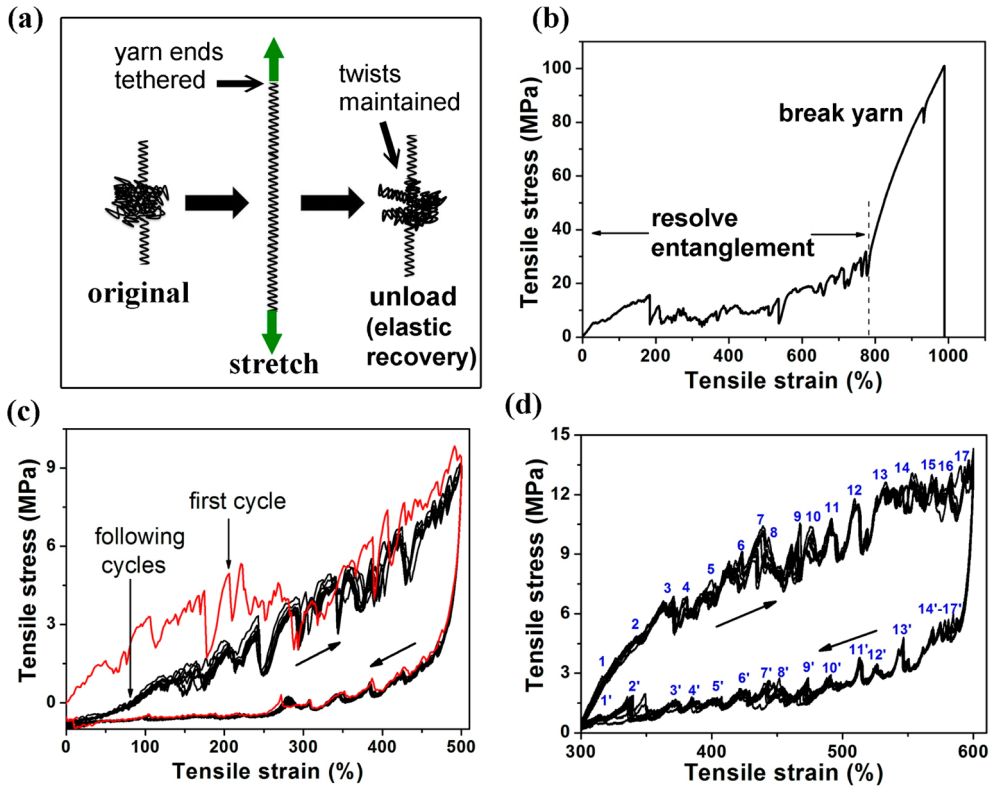

Figure 2. Mechanical properties of CNT entanglements. (a) Illustration of the experimental setup in which the two ends of an entanglement were tethered by grips (maintaining twists) and stretched uniaxially into predefined tensile strains for cyclic testing or until fracture. (b) Tensile stress−strain curve of a CNT entanglement showing a failure strain of 985% including two stages, a large strain range of twist resolving (ε = 0−800%) followed by a yarn breaking stage with rapidly increasing stress. (c) Stress−strain curves recorded over 10 cycles at maximum strain of 500%, showing that the first cycle behavior is different from the following cycles. (d) Stress−strain curves of an entanglement tested within ε = 300−600%, in which the stress peaks are labeled in the loading (1−17) and unloading stages (1′−17′).

control the twisting behavior at certain degree. Tensile tests on an entanglement to large strain (ε = 500%) for 600 cycles show repeating stress−strain curves, indicating its long-cycle ability without structural collapse (Figure S4).

To investigate the reversible structure change in more detail, an entanglement is stretched at a specific range (ε = 300−600%) for 20 cycles. The cyclic σ-ε curves reveal highly reproducible stress peaks (*e.g.*, peaks labeled as #11, #12) during both loading and unloading stages (Figure 2d). Some peaks during unloading (#11′, #13′) also have similar shape (although with reduced intensity) compared with those (#11, #13) during loading. The results indicate that a stable entangled structure is maintained during repeated stretching-releasing, and when a particular overtwisted point is unraveled (producing a distinct stress peak), the same structure can be recovered during unloading. Although the yarn entanglements are random and different from one to another, the resolving process of each entanglement is indeed very stable and reversible. Stress peaks in the unloading curve also imply that the entanglement returns to its original structure elastically, under the condition that the yarn ends are fixed by the grips to prevent releasing of internal twists. In addition, significant energy dissipation (due to friction between twisted segments) accompanies the resolving process, leading to large stress loops in every cycle.

The observed elastic behavior or CNT yarn entanglements is very suitable for applications such as large strain-range sensors (up to ε = 500%). Within this large strain, the entanglement can be stretched at different speeds (0.03−3 m/min) or strain rates (10−1000%/min) while producing similar $\sigma-\varepsilon$ curves (Figure 3a). It shows that the entanglement can be resolved at high speed with a stable behavior, which is useful for making stretchable sensors operating at high strain rates. Simultaneously recorded electrical resistance (R, measured across the entire yarn span) shows consistent change for nearly 600 strain cycles (Figure 3b). Although there are small fluctuations appearing in the resistance curve, a roughly linear relationship can be distinguished. The increase of R is probably due to the loss of physical contacts between twisted segments when they are resolved gradually. Furthermore, the relative resistance change ($\Delta R/R$) shows reproducible increase and decrease during 100 cycles, indicating very stable performance (Figure 3c). The resistance increases by 64% ($\Delta R/R \approx$ 64%) when the entanglement is

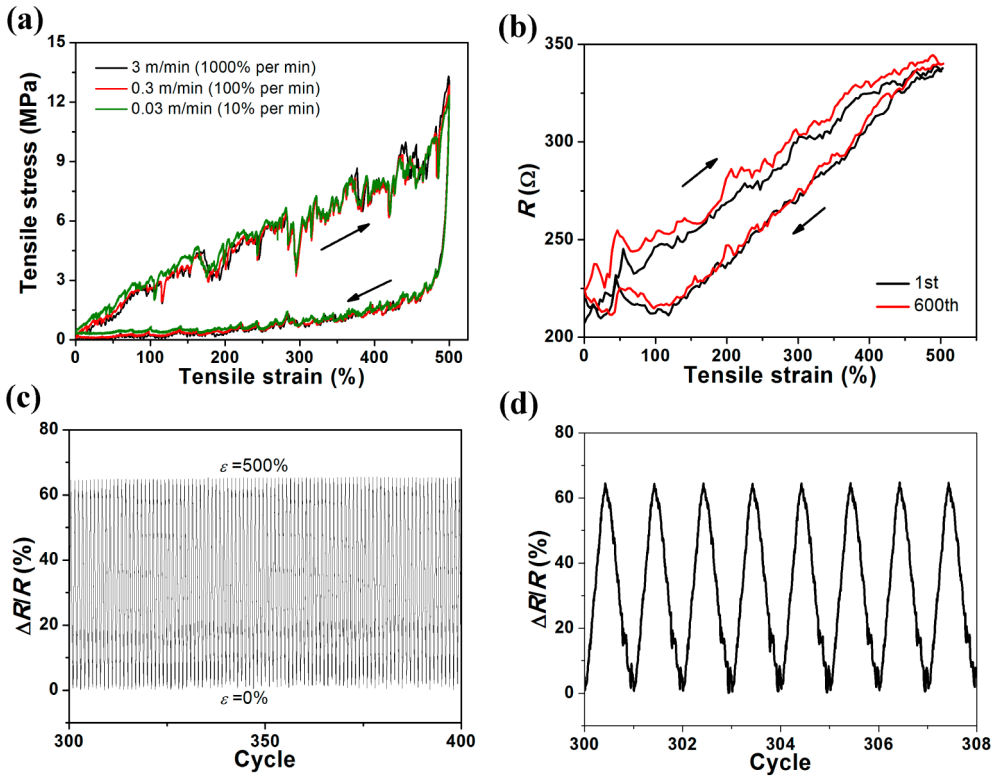

Figure 3. Large strain-range sensors based on CNT entanglements. (a) Stress−strain curves of an entanglement stretched by different speeds of 0.03, 0.3, and 3 m/min (corresponding to strain rates of 10, 100, and 1000%/min), respectively. (b) Simultaneously recorded electrical resistance during the first and 600th cycles, showing a roughly linear relationship. (c) Relative resistance change ($\Delta R/R$) for about 100 cycles showing highly reproducible and stable values at the stretched (ε = 500%) and recovered (ε = 0%) states. (d) Close view of $\Delta R/R$ for 8 cycles.

stretched to a strain of 500%, reversibly, demonstrating a large resistance change over a wide strain range (Figure 3d). The large operating range (ε = 500%) of our entangled yarns stems from the unique twist-resolving process, which can hardly be achieved from conventional CNT-based yarns or films.

Because the CNT entanglements store a large number of twists, it is possible to construct rotational actuators by controlled releasing of twists. To this end, we hang an object with certain weight (*e.g.*, a 3.3 g Al solid cylinder) to the yarn end, which applies a tensile stress (about 20 MPa) to the entanglement in a vertical setup (Figure 4a). This stress value is high enough to resolve the twists so that the attached object at the free end can be rotated continuously. During rotation, the entanglement is converted into a partially then fully resolved (straightened) yarn, with its length increasing and the cylinder height dropping gradually over time (Figure 4a,b). Different from previous methods in which the actuation is triggered by electric field or chemical agent, we directly utilize the tensile stress produced by a foreign object to realize twisting resolving and configure a mechanically driven actuator. We have recorded more than 1000 rotation cycles for several samples, and the actuation typically involves three stages including accelerating, stabilizing, and final degrading. Operating in air, the rotational speed reaches 915 rpm and then gradually drops to zero (Figure 4c). The platform region corresponding to maximum rotational speed occurs during the transition of an entanglement to a partially resolved yarn. After the entanglement has been fully resolved, one can twist it again into a similar morphology and use repeatedly. Slight degradation (decrease of cycle numbers) can be seen after three actuation cycles by the same yarn, however, the maximum rotational speed is maintained in 800−900 rpm for each cycle (Figure 4d). We have compared the same yarn spun in different morphologies (straight, single-helix, and complex entanglement), and the entanglement produces the largest rotational speed (Figure S5).

We find that the maximum speed generated by one yarn depends on the applied stress, therefore its actuating behavior can be tailored. The rotational speed increases with higher tensile stress because twists are resolved more rapidly, producing higher output energy density (Figure 4e). A lightweight CNT yarn (0.6 mg) can generate energy densities up to 8.3 J/g by calculating the kinetic energy (E) acquired in the rotating cylinder by

$$E = \frac{1}{2} J\omega^2 = \frac{1}{2}\left(\frac{1}{2} mr^2\right)\omega^2$$

where J is the moment of inertia, m is the mass of the cylinder (47 g), r is the cylinder radius (13 mm), and ω is

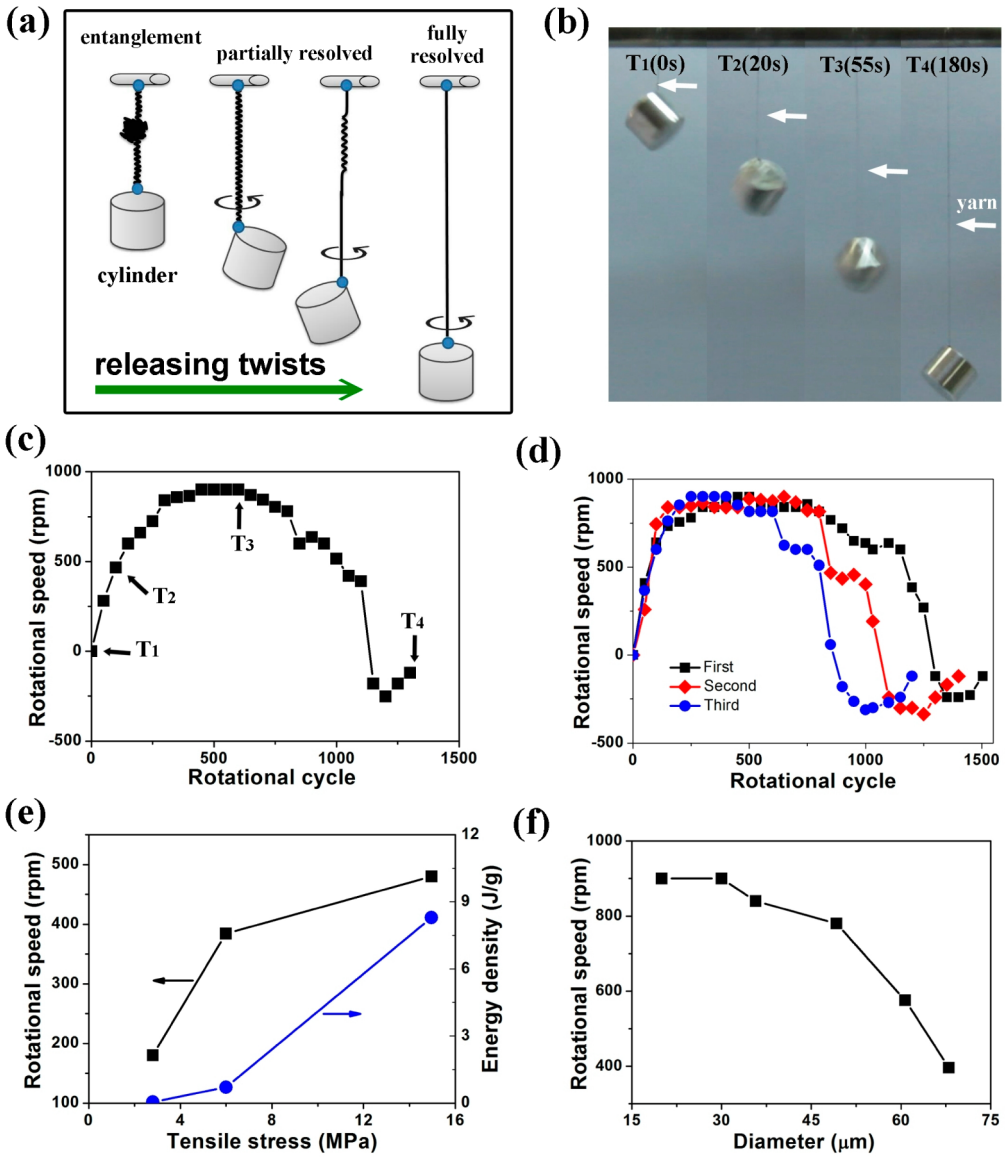

Figure 4. Rotational actuators based on CNT entanglements. (a) Illustration of the setup in which an entanglement was fixed to a horizontal rod at one end, and attached by a metal cylinder at the other free end. The tensile stress applied by the cylinder can resolve the twists within the entanglement and then rotate the cylinder, enabling rotational actuation. (b) Four snapshots on the rotating cylinder recorded during actuation. White arrows point to the CNT yarn. (c) Average rotational speed calculated during the entire actuation process, in which the metal cylinder has rotated for about 1300 cycles until complete stop. The four states (T_1–T_4) corresponding to the snapshots in (b) are labeled. (d) Rotational speed of an entanglement when it twists have been completely resolved and spun again for repeated use (3 times). (e) Rotational speeds of metal cylinders with different weights (producing different stress values in the yarn), showing increasing speed and energy density with higher stress. (f) Rotational speeds of the same metal cylinder (weight = 3.3 g) when it was actuated by yarns with different diameters (20–68 μm).

the maximum angular rotating speed (16π rad/s). The input energy is the decrease of potential energy (~0.028 J) of the cylinder (its height has dropped by 61 mm when reaching the maximum speed, see Figure 4b). This results in an energy conversion efficiency (from potential to kinetic energy) of about 18% given E = 0.005 J. Alternatively, we can control the yarn diameter to obtain different tensile stresses (under the same load) and tune the rotational speed (Figure 4f). For thicker yarns (diameter > 60 μm), the generated speed is relatively low (<600 rpm). Reducing the yarn diameter to less than 30 μm leads to rapid increase of the tensile stress within the yarn, resulting in significantly enhanced speed (~900 rpm). Currently, the energy density of our entangled yarns is comparable to previous electrically driven wax-infiltrated CNT yarns (1.36 J/g), while our mechanical actuation does not need electrical input. The performance (*e.g.*, speed, energy density) could be further improved by spinning thin CNT yarns with higher strength and reducing air friction during rotation.

CONCLUSIONS

In conclusion, we report the fabrication of over-twisted, resolvable CNT yarn entanglements with high

structural complexity. Owing to the presence of extensive twists, these entanglements can serve as elastic strain sensors over a wide strain range, and rotational actuators with high output energy density. Currently, the random entanglements show some general mechanical behavior such as large-strain stretching and rotational actuation, but such randomness would cause local fluctuations and performance instability in strain sensors and rotational actuators. Further study on the fabrication process and twisting mechanism might provide solutions on controlling the twisting position and yarn configuration, and reduce the influence of randomness. Twisted hierarchical yarn structures have various applications in micro and nano electromechanical systems, flexible and superstretchable devices, energy storage and conversion materials.

METHODS

Spinning of CNT Entanglements. The spinning process included the following steps. First, single-walled CNT films were synthesized by CVD with ferrocene and xylene as catalyst and carbon precursors at a reaction temperature of 1160 °C. The precursor solution (0.045 g/mL) with a small addition of sulfur (0.001 g/mL) was injected into the CVD furnace at a rate of 10 μL/min and carried by a gas mixture (Ar/H_2, volume ratio 0.85:0.15) at 1500 sccm into the reaction zone, typically for a period of 30 min. Second, an as-synthesized freestanding film (15 cm in length) was suspended horizontally with two ends fixed on an electric motor and a metal block (11.8 g), respectively. Third, the film was spun into a straight yarn at a motor speed of 100 rpm. Then, the straight yarn was spun into a single-helix yarn by continued overtwisting. Finally, the spinning was continued at a speed of about 20 rpm to further twist the yarn into an entanglement consisting of many double-helix segments. During the entire process, the metal block attached to one of the yarn end was moving smoothly toward the electric motor to allow the length shrinkage of the twisted yarn. The entanglement was removed from the motor and the block, and maintained a stable structure.

Structure Characterization and Mechanical Tests. The morphology and structure of the CNT entanglements before and after mechanical testing were characterized by SEM (Hitachi S4800). Mechanical tests were carried out in a single-column testing instrument (Instron 5843) equipped with a load cell of 10 N. The two ends of a CNT entanglement were fixed on a paper sheet with a cut window by polyvinyl alcohol as adhesive paint. This paper was installed into two grips aligned in a vertical setup. Then the paper was cut from its two sides to free the sample. For uniaxial tension tests, the entanglement was stretched at a constant speed of 1.0 mm/min until fracture. For cyclic tests, the stretching/releasing speed was set as 0.03−3 m/min within a strain range of 0−600%. Stress−strain curves were recorded simultaneously.

Electrical Measurements. The change of electrical resistance in the yarn was monitored simultaneously during mechanical testing. The two ends of a CNT entanglement were connected to electrical wires by silver paste. During cyclic tension tests, the current flow through the tested entanglement was also recorded by a source meter (Keithley 2635A) under a constant bias (0.1 V). The yarn resistance was calculated for the tested strain cycles.

Rotational Actuation. One end of the CNT entanglement was fixed on a suspended rod by polymer adhesive, and the other end was attached by a metal cylinder with certain weight (3.3−47.0 g). The setup can be seen as a cylinder hanging on a rod through a CNT yarn, with the lower end free to rotate. Under the tensile stress applied by the cylinder, the twisted entanglement started to resolve and simultaneously rotated the attached cylinder. The process of rotational actuation continued and the rotational speed of the cylinder increased to a maximum value, stabilized for a while, and then gradually dropped to zero. A digital camera was used to record the entire process and the rotational speed (revolutions per cycle) was calculated throughout the process.

Conflict of Interest: The authors declare no competing financial interest.

Acknowledgment. A. Cao acknowledges the Natural Science Foundation in China (NSFC program number 91127004) and the research found for the doctoral program of higher education (MOE 08600-452-10132-007). Y. Li acknowledges NSFC (11272109) and X. He acknowledges Ph.D. Programs Foundation of Ministry of Education of China (20122302110065).

Supporting Information Available: More SEM characterization on CNT entanglements made from different yarn diameters and before/after mechanical tests, longer cycle stress−strain curves, rotational actuation results of different yarn configurations. This material is available free of charge *via* the Internet at http://pubs.acs.org.

REFERENCES AND NOTES

1. Vigolo, B.; Pénicaud, A.; Coulon, C.; Sauder, C.; Pailler, R.; Journet, C.; Bernier, P.; Poulin, P. Macroscopic Fibers and Ribbons of Oriented Carbon Nanotubes. *Science* **2000**, *290*, 1331–1334.
2. Jiang, K.; Li, Q.; Fan, S. Spinning Continuous Carbon Nanotube Yarns. *Nature* **2002**, *419*, 801.
3. Ericson, L. M.; Fan, H.; Peng, H.; Davis, V. A.; Zhou, W.; Sulpizio, J.; Wang, Y. H.; Booker, R.; Vavro, J.; Guthy, C.; *et al.* Macroscopic, Neat, Single Walled Carbon Nanotube Fibers. *Science* **2004**, *305*, 1447–1450.
4. Li, Y. L.; Kinloch, I. A.; Windle, A. H. Direct Spinning of Carbon Nanotube Fibers from Chemical Vapor Deposition Synthesis. *Science* **2004**, *304*, 276–278.
5. Zhang, M.; Atkinson, K. R.; Baughman, R. H. Multifunctional Carbon Nanotube Yarns by Downsizing an Ancient Technology. *Science* **2004**, *306*, 1358–1361.
6. Koziol, K.; Vilatela, J.; Moisala, A.; Motta, M.; Cunniff, P.; Sennett, M.; Windle, A. High-Performance Carbon Nanotube Fiber. *Science* **2007**, *318*, 1892–1895.
7. Zhang, X. B.; Jiang, K. L.; Teng, C.; Liu, P.; Zhang, L.; Kong, J.; Zhang, T. H.; Li, Q. Q.; Fan, S. S. Spinning and Processing Continuous Yarns from 4-in. Wafer Scale Super-Aligned Carbon Nanotube Arrays. *Adv. Mater.* **2006**, *18*, 1505–1510.
8. Dalton, A. B.; Collins, S.; Munoz, E.; Razal, J. M.; Ebron, V. H.; Ferraris, J. P.; Coleman, J. N.; Kim, B. G.; Baughman, R. H. Super-Tough Carbon-Nanotube Fibres. *Nature* **2003**, *423*, 703.
9. Behabtu, N.; Young, C. C.; Tsentalovich, D. E.; Kleinerman, O.; Wang, X.; Ma, A. W. K.; Bengio, E. A.; ter Waarbeek, R. F.; deJong, J. J.; Hoogerwerf, R. E.; *et al.* Strong, Light, Multifunctional Fibers of Carbon Nanotubes with Ultrahigh Conductivity. *Science* **2013**, *339*, 182–185.
10. Zhao, Y.; Wei, J. Q; Vajtai, R.; Ajayan, P. M.; Barrera, E. V. Iodine Doped Carbon Nanotube Cables Exceeding Specific Electrical Conductivity of Metals. *Sci. Rep.* **2011**, *1*, 83.
11. Zhao, H.; Zhang, Y.; Bradford, P. D.; Zhou, Q.; Jia, Q.; Yuan, F.-G.; Zhu, Y. Carbon Nanotube Yarn Strain Sensors. *Nanotechnology* **2010**, *21*, 305502.
12. Zhang, S.; Ji, C.; Bian, Z.; Yu, P.; Zhang, L.; Liu, D.; Shi, E.; Shang, Y.; Peng, H.; Cheng, Q.; *et al.* Porous, Platinum Nanoparticle-Adsorbed Carbon Nanotube Yarns for Efficient Fiber Solar Cells. *ACS Nano* **2012**, *8*, 7191–7198.
13. Liu, D.; Zhao, M.; Li, Y.; Bian, Z.; Zhang, L.; Shang, Y.; Xia, X.; Zhang, S.; Yun, D.; Liu, Z.; *et al.* Solid-State, Polymer-Based Fiber Solar Cells with Carbon Nanotube Electrodes. *ACS Nano* **2012**, *6*, 11027–11034.

14. Foroughi, J.; Spinks, G. M.; Wallace, G. G.; Oh, J.; Kozlov, M. E.; Fang, S. L.; Mirfakhrai, T.; Madden, J. D. W.; Shin, M. K.; Kim, S. J.; *et al.* Torsional Carbon Nanotube Artificial Muscles. *Science* **2011**, *334*, 494–497.
15. Guo, W.; Liu, C.; Zhao, F.; Sun, X.; Yang, Z.; Chen, T.; Chen, X.; Qiu, L. B.; Hu, X.; Peng, H. S. A Novel Electromechanical Actuation of Carbon Nanotube Fiber. *Adv. Mater.* **2012**, *24*, 5379–5384.
16. Chen, T.; Qiu, L. B.; Yang, Z.; Cai, Z. B.; Ren, J.; Li, H.; Lin, H.; Sun, X.; Peng, H. S. An Integrated Energy Wire for Both Photoelectric Conversion and Storage. *Angew. Chem., Int. Ed.* **2012**, *51*, 11977–11980.
17. Chen, T.; Qiu, L. B.; Cai, Z. B.; Gong, F.; Yang, Z.; Wang, Z.; Peng, H. S. Intertwined Aligned Carbon Nanotube Fiber Based Dye-Sensitized Solar Cells. *Nano Lett.* **2012**, *12*, 2568–2572.
18. Ren, J.; Li, L.; Chen, C.; Chen, X. L.; Cai, Z. B.; Qiu, L. B.; Wang, Y. G.; Zhu, X. R.; Peng, H. S. Twisting Carbon Nanotube Fibers for Both Wire-Shaped Micro-Supercapacitor and Micro-Battery. *Adv. Mater.* **2013**, *25*, 1155–1159.
19. Lima, M. D.; Li, N.; Andrade, M. J.; Fang, S. L.; Oh, J. Y.; Spinks, G. M.; Kozlov, M. E.; Haines, C. S.; Suh, D. S.; Foroughi, J.; *et al.* Electrically, Chemically, and Photonically Powered Torsional and Tensile Actuation of Hybrid Carbon Nanotube Yarn Muscles. *Science* **2012**, *338*, 928–932.
20. Shang, Y.; He, X.; Li, Y.; Zhang, L.; Li, Z.; Ji, C.; Shi, E.; Li, P.; Zhu, K.; Peng, Q.; *et al.* Super-Stretchable Spring-Like Carbon Nanotube Ropes. *Adv. Mater.* **2012**, *24*, 2896–2900.
21. Shang, Y.; Li, Y.; He, X.; Zhang, L.; Shi, E.; Wu, S.; Li, Z.; Li, P.; Wei, J.; Wang, K.; *et al.* Highly Twisted Double-Helix Carbon Nanotube Yarns. *ACS Nano* **2013**, *7*, 1446–1453.